

AN OPTIMIZATION-BASED MODEL ORDER REDUCTION APPROACH FOR COUPLED PROBLEMS: APPLICATION TO THERMO-HYDRO-MECHANICAL SYSTEMS

A. IOLLO[†], G. SAMBATARO* AND T. TADDEI[†]

[†] IMB, UMR 5251, Université de Bordeaux, France;
Inria Bordeaux South-West, MEMPHIS team, France.

*Université Paris Est, CERMICS (ENPC);
Inria Paris, MATHERIALS team, France.

Key words: model order reduction, domain decomposition, coupled problems.

Abstract. In this work we develop a component-based model order reduction (CB-pMOR) procedure for a class of problems in nonlinear mechanics with internal variables. The work is motivated by applications to thermo-hydro-mechanical (THM) systems for radioactive waste disposal. The THM system is coupled, time-dependent, and highly nonlinear; furthermore, the solution to the problem depends on several parameters, which might be related to the geometric configuration (e.g. the number of repositories, their distance or their size) or the material properties of the medium. We investigate the effectiveness of the proposed method in terms of accuracy and computational costs for a two-dimensional THM system in the case of overlapping partitions.

1 Introduction

Standard computational methods based on a high-fidelity (HF) discretization of parameterized partial differential equation (PDEs) often require prohibitively large computational costs to achieve sufficiently accurate numerical solutions for *real-time* and *many-query* applications that naturally arise for a wide range of problems in science and engineering. To address this issue, parametric model order reduction (pMOR) techniques build a low-dimensional model, which requires short simulation times and low data storage, but still keeps the approximation error between the reduced-order solution and the HF solution under control. The reduced basis (RB, [4, 11]) method obtains a solution through the projection of the HF problem onto a small subspace, which is constructed in a *training* stage for the specific problem at hand. Standard pMOR techniques rely on HF solves at training stage, which might be unaffordable for very large-scale problems; furthermore, standard pMOR techniques rely on the assumption that the solution field is defined over a parameter-independent domain or over a family of diffeomorphic domains. The objective of this paper is to devise a component-based pMOR procedure for large-scale problems in mechanics, with emphasis on thermo-hydro-mechanical (THM) systems.

We introduce the spatial variable x in the Lipschitz domain $\Omega \subset \mathbb{R}^d$ with dimension $d = 2, 3$, and the time variable t in the time interval $(0, t_f] \subset \mathbb{R}$, where t_f is the final time. We further define the vector of parameters μ in the compact parameter region $\mathcal{P} \subset \mathbb{R}^P$. Given a parameter

$\mu \in \mathcal{P}$, we introduce the vector of D state (or primary) variables $\underline{U}_\mu : \Omega \times (0, t_f] \rightarrow \mathbb{R}^D$; we also introduce D_{cl} internal (or dependent) variables $\underline{W}_\mu : \Omega \times (0, t_f] \rightarrow \mathbb{R}^{D_{\text{cl}}}$. We denote by \mathcal{X} and \mathcal{W} suitable Hilbert spaces in Ω for \underline{U}_μ and \underline{W}_μ , respectively. We denote by (w, v) the inner product in \mathcal{X} for all $w, v \in \mathcal{X}$, and by $\|w\| = \sqrt{(w, w)}$ the induced norm. We denote by \mathcal{X}_0 the test set such that $\mathcal{X}_0 = \{v \in \mathcal{X} : v|_{\Gamma_{\text{dir}}=0}\}$, where Γ_{dir} denotes the portion of the boundary associated with Dirichlet boundary conditions; we denote the time derivative as $\partial_t \underline{U}_\mu \in L^2(0, t_f; \mathcal{X}_0^{-1})$. Then, we introduce the PDE problem

$$\begin{cases} \mathcal{R}(\underline{U}_\mu, \partial_t \underline{U}_\mu, \underline{W}_\mu; v, \mu) = 0, & \forall v \in \mathcal{X}_0, \quad t \in (0, t_f], \\ \dot{\underline{W}}_\mu = \mathcal{F}(\underline{U}_\mu, \underline{W}_\mu; \mu), & \text{in } \Omega \times (0, t_f], \end{cases} \quad (1)$$

The form \mathcal{R} is associated to a nonlinear second-order in space, first-order in time differential operator that is associated with the equilibrium equations, while \mathcal{F} is a set of ordinary differential equations (ODEs) that is associated with the constitutive laws.

We are interested in the prediction of the long-term behavior of temperature, pore water pressure and solid displacement in the neighborhood of geological repositories for radioactive waste disposal. Radioactive waste is placed in elongated repositories that are located deep underground ($\approx 300 - 500$ [m]) and are responsible for a significant thermal flux towards the Earth's surface. The problem is modeled by the THM equations, which can be written in the form (1). Typical parameters involve material properties, boundary conditions (e.g., the thermal flux associated with each repository), and the number of repositories Q_a (cf. Figure 1(a)). We refer to [7] for a detailed description of the problem of interest.

Changes in the number of repositories Q_a induce a topology change in the computational domain that prevents the definition of a single reference configuration for all parameters and thus the application of standard pMOR methods; we should hence develop CB-pMOR techniques [6].

During the offline stage, a library of *archetype components* is defined, and local reduced-order bases (ROBs) as well as local ROMs are built; then, during the online stage, local components are instantiated to form the global system and the global solution is estimated by coupling local ROMs. In Figure 1(b), we show how to decompose the global domain Ω considered in the numerical experiments into an overlapping partition $\{\Omega_i\}_{i=1}^{N_{\text{dd}}}$ for a given value of the geometric parameter Q_a ; next to the instantiated subdomains, we depict the two archetype components ("internal" and "external") of the library.

CB-pMOR strategies consist of two distinct building blocks: (i) a rapid and reliable domain decomposition (DD) strategy for online global predictions, and (ii) a localized training strategy exclusively based on local solves for the construction of the local approximations. In this work, we focus exclusively on (i); we refer to [1, 5, 13] for recent works on localized training for nonlinear elliptic PDEs. Our work builds upon the component-based pMOR procedure dubbed one-shot overlapping Schwarz (OS2) and proposed in [8] for steady PDEs. The key features of the OS2 approach are twofold: (i) a constrained optimization statement that penalizes the jump at the components' interfaces subject to the approximate satisfaction of the PDE in each instantiated component; (ii) the decomposition of the local solutions into a *port component* — associated with the solution on interior boundaries (*ports*) — and a *bubble component* that vanishes at *ports*, to enable effective parallelization of the online solver. Our optimization statement might be interpreted as the limit of standard (multiplicative or additive) overlapping

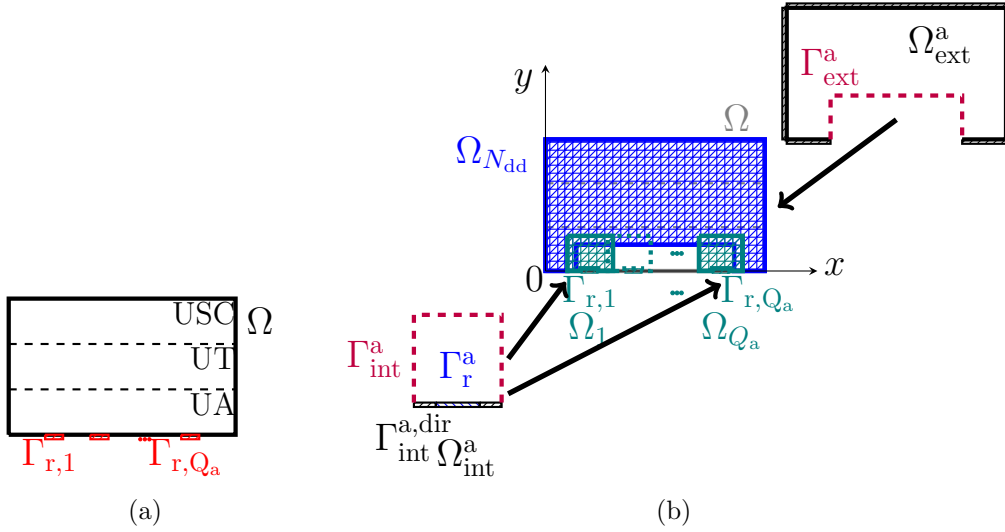


Figure 1: (a) domain Ω and boundaries $\Gamma_{r,1}, \dots, \Gamma_{r,Q_a}$ associated to the repositories. In the vertical (y) direction, the domain is split into three layers: a clay layer denoted as UA (“unité argilleuse”), a transition layer UT (“unité de transition”) and a silt-carbonate layer USC (“unité silto-carbonatée”); (b) overlapping partition used for CB-pMOR.

Schwarz (OS) methods: rather than performing alternate local solves in each subdomain, we directly tackle the limit formulation.

2 Formulation

We discuss below the DD formulation of the THM problem (1). Due to the page limit, we do not provide a detailed description of the PDE model and the temporal discretization. We refer to [7] and [12] for a thorough presentation of the continuous and discrete models: the detailed formulation of the THM continuous problem can be found in [7] in section 4.2 (both the equilibrium equations (23a) – (26) and the constitutive laws (27a) – (27e) are introduced), together with the boundary conditions at Eqs. (23a), (24a), (25a); the discrete model is presented in section 4.3 (at Eqs. (31) – (32)).

2.1 Archetype components

We use the superscript $(\cdot)^a$ to indicate quantities and spaces defined for a given archetype component; we further denote by ℓ a generic element of the library \mathcal{L} of archetype components. We define the archetype components $\{\Omega_\ell^a\}_{\ell \in \mathcal{L}} \subset \mathbb{R}^d$; we denote by Γ_ℓ^a the portion of $\partial\Omega_\ell^a$ that lies inside the computational domain (“port”) (marked in purple in Figure 1(b)). For each archetype component $\ell \in \mathcal{L}$, we define the local discrete high-fidelity (HF) finite element (FE) space $\mathcal{X}_\ell^a \subset [H_{0,\Gamma_\ell^a,dir}^1(\Omega_\ell^a)]^D$, the bubble space $\mathcal{X}_{\ell,0}^a = \{v \in \mathcal{X}_\ell^a : v|_{\Gamma_\ell^a} = 0\}$, and the port space $\mathcal{U}_\ell^a = \{v|_{\Gamma_\ell^a} : v \in \mathcal{X}_\ell^a\} \subset [H^{1/2}(\Gamma_\ell^a)]^D$. We endow \mathcal{X}_ℓ^a with the inner product $(\cdot, \cdot)_\ell$ and the induced norm $\|\cdot\|_\ell = \sqrt{(\cdot, \cdot)_\ell}$, we define $N_\ell^a = \dim(\mathcal{X}_\ell^a)$, and the extension operator $\mathbf{E}_\ell^a : \mathcal{U}_\ell^a \rightarrow \mathcal{X}_\ell^a$ such that

$$(\mathbf{E}_\ell^a w, v)_\ell = 0 \quad \forall v \in \mathcal{X}_{\ell,0}^a, \quad \mathbf{E}_\ell^a w|_{\Gamma_\ell^a} = w, \quad \forall w \in \mathcal{U}_\ell^a. \quad (2)$$

We define the vector of local parameters μ_ℓ in the parameter region \mathcal{P}_ℓ , which include geometric and material parameters that identify the physical model in any instantiated component of type ℓ . Furthermore, for any $\ell \in \mathcal{L}$, we define the parametric mapping $\Phi_\ell^a : \Omega_\ell^a \times \mathcal{P}_\ell \rightarrow \mathbb{R}^d$ that describes the deformation of the archetype component ℓ for the parameter value $\mu_\ell \in \mathcal{P}_\ell$.

We resort to an implicit Euler time discretization scheme based on the time grid $\{t^{(j)}\}_{j=1}^{J_{\max}}$ for the non-dimensional time interval $(0, t_f]$, with $t_f = 1$. We denote by $\underline{U}^{(j)}$ and $\underline{W}^{(j)}$ the estimates of the state and internal variables at time t_j , for $j = 1, \dots, J_{\max}$. Given parameter $\mu_\ell \in \mathcal{P}$, for $\ell \in \mathcal{L}$, we define the time-discrete variational form $\mathcal{R}_\ell^{a,(j)} : \mathcal{X}_\ell^a \times \mathcal{X}_{\ell,0}^a \times \mathcal{P}_\ell \rightarrow \mathbb{R}$ associated with the ℓ^{th} archetype component:

$$\begin{aligned} \mathcal{R}_\ell^{a,(j)}(\underline{U}^{(j)}, \underline{v}; \mu_\ell) &= \mathcal{R}_\ell^a(\underline{U}^{(j)}, \underline{U}^{(j-1)}, \underline{W}^{(j)}, \underline{W}^{(j-1)}, \underline{v}; \mu_\ell) \\ &= \sum_{k=1}^{N_\ell^e} \int_{\mathcal{D}_{\ell,k}} \eta_\ell^{a,e}(\underline{U}^{(j)}, \underline{U}^{(j-1)}, \underline{W}^{(j)}, \underline{W}^{(j-1)}, \underline{v}; \mu_\ell) dx \\ &\quad + \int_{\partial \mathcal{D}_{\ell,k}} \eta_\ell^{a,f}(\underline{U}^{(j)}, \underline{U}^{(j-1)}, \underline{W}^{(j)}, \underline{W}^{(j-1)}, \underline{v}; \mu_\ell) dx, \end{aligned} \quad (3)$$

where $\{\mathcal{D}_{\ell,k}\}_{k=1}^{N_\ell^e}$ denote the elements of the FE mesh for the archetype component Ω_ℓ^a ; dependence on the geometry is embedded in the local forms $\eta_\ell^{a,e}, \eta_\ell^{a,f}$, which involve the mapping Φ_ℓ^a . To simplify the notation, we omit the subscript μ on state solutions and internal variables and we omit the dependence of the variational forms on the parameters.

2.2 Instantiated system

A physical system is uniquely described by a set of N_{dd} labels $\{\mathbf{L}_i\}_{i=1}^{N_{\text{dd}}} \subset \mathcal{L}$, and the set of parameters $\mu := (\mu_1, \dots, \mu_{N_{\text{dd}}}) \in \mathcal{P} := \bigotimes_{i=1}^{N_{\text{dd}}} \mathcal{P}_{\mathbf{L}_i}$. Given $\mu \in \mathcal{P}$, we define

- (i) the mappings $\{\Phi_i\}_{i=1}^{N_{\text{dd}}}$ such that $\Phi_i = \Phi_{\mathbf{L}_i}^a(\cdot; \mu_i)$ for $i = 1, \dots, N_{\text{dd}}$;
- (ii) the instantiated overlapping partition $\{\Omega_i = \Phi_i(\Omega_{\mathbf{L}_i}^a)\}_{i=1}^{N_{\text{dd}}}$, the global open domain $\Omega \subset \mathbb{R}^d$ such that $\bar{\Omega} = \bigcup_i \bar{\Omega}_i$, the ports $\Gamma_i = \Phi_i(\Gamma_{\mathbf{L}_i}^a)$ and the Dirichlet boundaries $\Gamma_i^{\text{dir}} = \Phi_i(\Gamma_{\mathbf{L}_i}^{a,\text{dir}})$, for $i = 1, \dots, N_{\text{dd}}$;
- (iii) the deployed FE full, bubble, and port spaces $\mathcal{X}_i = \{v \circ \Phi_i^{-1} : v \in \mathcal{X}_{\mathbf{L}_i}^a\}$, $\mathcal{X}_{i,0} = \{v \circ \Phi_i^{-1} : v \in \mathcal{X}_{\mathbf{L}_i,0}^a\}$, and $\mathcal{U}_i = \{v|_{\Gamma_i} : v \in \mathcal{X}_i\}$, for $i = 1, \dots, N_{\text{dd}}$;
- (iv) the extension operators $\mathbf{E}_i : \mathcal{U}_i \rightarrow \mathcal{X}_i$ such that $\mathbf{E}_i w = \mathbf{E}_{\mathbf{L}_i}^a(w \circ \Phi_i) \circ \Phi_i^{-1}$ for $i = 1, \dots, N_{\text{dd}}$;
- (v) the deployed variational forms $\mathcal{R}_i^{(j)} : \mathcal{X}_i \times \mathcal{X}_{i,0} \rightarrow \mathbb{R}$ such that

$$\mathcal{R}_i^{(j)}(w, v) = \mathcal{R}_{\mathbf{L}_i}^{a,(j)}(w \circ \Phi_i, v \circ \Phi_i; \mu_i). \quad (4)$$

Given $i = 1, \dots, N_{\text{dd}}$, we further define the set of neighboring elements $\text{Neigh}_i = \{j : \Omega_j \cap \Omega_i \neq \emptyset, j \neq i\}$, and denote the partition of Γ_i as $\{\Gamma_{i,j} = \Gamma_i \cap \Omega_j : j \in \text{Neigh}_i\}$ — note that $\Gamma_{i,j} \neq \Gamma_{j,i}$.

Given the archetype mesh $\mathcal{T}_\ell^a = \left(\{x_{\ell,j}^{a,v}\}_{j=1}^{N_\ell^v}, \mathbf{T}_\ell\right)$, with nodes $\{x_{\ell,j}^{a,v}\}_{j=1}^{N_\ell^v}$, connectivity matrix \mathbf{T}_ℓ and elements $\{\mathcal{D}_{k,\ell}\}_{k=1}^{N_\ell^e}$, we denote by U a generic element of \mathcal{X}_ℓ and we denote by

$\mathbf{U} \in \mathbb{R}^{DN_\ell}$ the corresponding FE vector associated with the Lagrangian basis of \mathcal{T}_ℓ^a , for all $\ell \in \mathcal{L}$. Following [14], we pursue a discretize-then-map treatment of parameterized geometries: given the mesh $\mathcal{T}_{L_i}^a$, we state the local variational problems in the deformed mesh $\Phi_i(\mathcal{T}_{L_i}^a) = \left(\{\Phi_i(x_{j,L_i}^{a,v})\}_{j=1}^{N_{L_i}^a}, \mathbf{T}_{L_i} \right)$. Note that if $(\mathcal{T}_\ell^a, \mathbf{U})$ is associated with the element $U \in \mathcal{X}_\ell$, then $(\Phi_i(\mathcal{T}_\ell^a), \mathbf{U})$ approximates $U \circ \Phi^{-1}$.

2.3 Variational formulation

We denote as \underline{U}_i the trajectory associated with solution $\{\underline{U}_i^{(j)}\}_{j=1}^{J_{\max}}$ for each instantiated component $i = 1, \dots, N_{\text{dd}}$. Given the set of parameters $\mu = (\mu_1, \dots, \mu_{N_{\text{dd}}}) \in \mathcal{P}$, we seek the global solution trajectory $\vec{\underline{U}} = \{\underline{U}_1, \dots, \underline{U}_{N_{\text{dd}}}\} \subset \mathcal{X} = \bigotimes_{i=1}^{N_{\text{dd}}} \mathcal{X}_i$ such that (for each $j = 1, \dots, J_{\max}$) $\vec{\underline{U}} = \{\underline{U}_1^{(j)}, \dots, \underline{U}_{N_{\text{dd}}}^{(j)}\}$ solves the following constrained problem:

$$\begin{aligned} \min_{\vec{\underline{U}} \subset \mathcal{X}} & \frac{1}{2} \sum_{i=1}^{N_{\text{dd}}} \sum_{k \in \text{Neigh}_i} \|\underline{U}_i^{(j)} - \underline{U}_k^{(j)}\|_{L^2(\Gamma_{i,k})}^2 \\ \text{s.t.} & \begin{cases} \mathcal{R}_i^{(j)}(\underline{U}_i^{(j)}, \underline{V}) = 0 \\ \underline{W}_i^{(j)} = \mathcal{F}^{(j)}(\underline{U}_i^{(j)}, \underline{U}_i^{(j-1)}, \underline{W}_i^{(j-1)}) \end{cases} \quad \text{for } i = 1, \dots, N_{\text{dd}}. \end{aligned} \quad (5)$$

Remark 1. *The proposed optimization-based formulation is the limit of the (multiplicative or additive) OS method, as clarified in [8, section 1.2], for a steady PDE problem. Indeed, if we neglect the errors due to the local FE discretization, convergence of OS to a limit state $(U_1^*, \dots, U_{N_{\text{dd}}}^*)$ necessarily implies $\|U_i^{*(j)} - U_k^{*(j)}\|_{L^2(\Gamma_i \cup \Gamma_k)} = 0$ for each couple of instantiated subdomains $i, k = 1, \dots, N_{\text{dd}}$ and each time step $j = 1, \dots, J_{\max}$. This observation motivates the minimization of the jump of subsolutions at components' interfaces in the one-shot formulation (5).*

Remark 2. *In the objective function in (5) the jumps of solutions at components' interfaces only involve the state variables. The internal variables only come into play in the solution to the local problems (cf. the constraints in (5)) at each subdomain Ω_i , for $i = 1, \dots, N_{\text{dd}}$. Hence, the OS2 formulation can be conveniently applied to systems with a large number of constitutive laws and internal variables.*

2.4 Reduced-order formulation

We recast the constrained problem (5) into an unconstrained problem through the procedure described in [8]. We introduce the port state variables $\underline{U}_{p,i}^{(j)} \in \mathcal{U}_i$ as the restriction of local solutions $\underline{U}_i^{(j)}$ to the corresponding ports, and the internal variables $\underline{W}_i^{(j)} \in \mathcal{W}_i$. We define the port-to-bubble maps for problems of type (3) and for each instantiated component $i = 1, \dots, N_{\text{dd}}$ as $\mathbf{F}_i^{(j)} : \mathcal{U}_i \rightarrow \mathcal{X}_{i,0}$ as follows: given local port solutions $\underline{U}_{p,i}^{(j)}$ for each time step $j = 1, \dots, J_{\max}$,

$$\mathcal{R}_i^{(j)}\left(\mathbf{F}_i^{(j)}\left(\underline{U}_{p,i}^{(j)}\right) + \mathbf{E}_i\left(\underline{U}_{p,i}^{(j)}, \underline{v}\right)\right) = 0 \quad \forall \underline{v} \in \mathcal{X}_{i,0} \quad (6)$$

for $j = 1, \dots, J_{\max}$. A local solution can indeed be written as

$$\underline{U}_i^{(j)} = \mathbf{F}_i^{(j)}\left(\underline{U}_{p,i}^{(j)}\right) + \mathbf{E}_i\left(\underline{U}_{p,i}^{(j)}\right) \quad (7)$$

for $i = 1, \dots, N_{\text{dd}}$. Equation (6) corresponds to a time discretization of a localized PDE problem with $\underline{U}_{\text{p},i}^{(j)}$ as a datum on the port boundary Γ_i at time $t^{(j)}$. The unconstrained formulation reads: find $\underline{\hat{U}}_{\text{p}} = (\underline{U}_{\text{p},1}, \dots, \underline{U}_{\text{p},N_{\text{dd}}})$ that solves, for each $j = 1, \dots, J_{\text{max}}$,

$$\min_{\underline{U}_{\text{p}} \subset \mathcal{U}} \frac{1}{2} \sum_{i=1}^{N_{\text{dd}}} \sum_{k \in \text{Neigh}_i} \left\| \underline{U}_{\text{p},i}^{(j)} - \mathbf{E}_k \left(\underline{U}_{\text{p},k}^{(j)} \right) - \mathbf{F}_k^{(j)} \left(\underline{U}_{\text{p},k}^{(j)} \right) \right\|_{L^2(\Gamma_{i,k})}^2 \quad (8)$$

where $\mathcal{U} = \bigotimes_{i=1}^{N_{\text{dd}}} \mathcal{U}_i$. To introduce a low-dimensional reduced-order approximation, we rely on Galerkin projection of the port-to-bubble maps. We refer to [8], section 2.3.2, for the discussion about the construction of local low-dimensional archetype bubble and port spaces and the statement of a reduced-order formulation of (8). We notice that the procedure described in [8, section 2.3.2] easily generalizes to time-dependent coupled problems: notice that the minimization formulation holds for each time step $j = 1, \dots, J_{\text{max}}$; also, the constraints in (5) are associated with a time-dependent coupled problem rather than a steady one. We denote reduced port coefficients as $\hat{\beta}_i : \mathcal{P} \times (0, t_f] \rightarrow \mathbb{R}^m$ and we define the vector of assembled port coefficients as $\beta = [\beta_1, \dots, \beta_{N_{\text{dd}}}] \in \mathbb{R}^M$, with the total dimension of the assembled port space as $M = mN_{\text{dd}}$.

The bubble reduced coefficients are denoted as $\hat{\alpha}_i : \mathcal{P} \times (0, t_f] \rightarrow \mathbb{R}^n$ and are s.t. $\alpha_i^{(j)} = \hat{\mathbf{F}}_i^{(j)}(\beta_i^{(j)})$, where the total dimension of the assembled bubble space is denoted as $N = nN_{\text{dd}}$.

We report the low-dimensional OS2 statement: for each time step $j = 1, \dots, J_{\text{max}}$, find $\hat{\beta} = [\hat{\beta}_1, \dots, \hat{\beta}_{N_{\text{dd}}}] \in \mathbb{R}^M$ such that

$$\hat{\beta} \in \arg \min_{\beta \in \mathbb{R}^M} \frac{1}{2} \sum_{i=1}^{N_{\text{dd}}} \sum_{k \in \text{Neigh}_i} \left\| \underline{Z}_i^{\text{p}} \beta_i^{(j)} - \underline{Z}_k^{\text{p}} \beta_k^{(j)} - \underline{Z}_k^{\text{b}} \hat{\mathbf{F}}_k^{(j)} \left(\beta_k^{(j)} \right) \right\|_{L^2(\Gamma_{i,k})}^2. \quad (9)$$

As in [8], we can write problem (9) as

$$\hat{\beta} \in \arg \min_{\beta \in \mathbb{R}^M} \frac{1}{2} \|\mathbf{r}^{(j)}(\beta)\|_2^2 \quad (10)$$

where $\mathbf{r}^{(j)}(\beta) = \mathbf{P} \hat{\mathbf{F}}^{(j)}(\beta) + \mathbf{Q} \beta$ for suitable linear operators \mathbf{P} and \mathbf{Q} .

As for the application of hyper-reduction methods for the efficient approximation of local port-to-bubble maps, we refer to [8, section 2.3.2].

3 Solution to OS2 minimization problem

We describe in Algorithm 1 the overall procedure, which relies on Gauss-Newton method, to solve the unconstrained low-dimensional problem (9). The computation of the initial conditions for the THM problem is discussed in [7, section 4.2.1] and [12, section 6.2.3].

We observe that the internal for-loop block from line 4 to line 14 corresponds to block 3 – 13 in Algorithm 2 in [8]; here we extend the iterative procedure due to the need to i) update state and internal variables at each time step j (cf. line 15), ii) update the reduced port coefficients (cf. line 18). The Jacobian of the global port-to-bubble map is $\hat{\mathbf{F}}^{(j)} : \mathbb{R}^M \rightarrow \mathbb{R}^N$ is

Algorithm 1 Solution to (9) through the Gauss-Newton method.

Inputs: $\boldsymbol{\alpha}^{(0)} = [\boldsymbol{\alpha}_1^{(0)}, \dots, \boldsymbol{\alpha}_{N_{\text{dd}}}^{(0)}]$, $\boldsymbol{\beta}^{(0)} = [\boldsymbol{\beta}_1^{(0)}, \dots, \boldsymbol{\beta}_{N_{\text{dd}}}^{(0)}]$ initial conditions, $\mathbf{U}^{(0)}$, $\mathbf{W}^{(0)}$, $tol > 0$, maxit , J_{max} .

Outputs: $\left\{ \hat{\mathbf{U}}_1^{(j)} \right\}_{j=1}^{J_{\text{max}}}, \dots, \left\{ \hat{\mathbf{U}}_{N_{\text{dd}}}^{(j)} \right\}_{j=1}^{J_{\text{max}}}$.

- 1: Compute the matrices \mathbf{P}, \mathbf{Q} in (10).
 - 2: Set $\hat{\boldsymbol{\beta}}^{(0)} = \boldsymbol{\beta}^{(0)}$ and $\hat{\boldsymbol{\alpha}} = \boldsymbol{\alpha}^{(0)}$.
 - 3: **for** $j = 1, \dots, J_{\text{max}}$ **do**
 - 4: **for** $k = 1, \dots, \text{maxit}$ **do**
 - 5: **for** $i = 1, \dots, N_{\text{dd}}$ **do**
 - 6: Solve $\hat{\mathbf{R}}_i^{(j)}(\boldsymbol{\alpha}_i, \boldsymbol{\beta}_i^{(k)}) = \mathbf{0}$ using Newton's method with initial condition $\hat{\boldsymbol{\alpha}}_i$.
 - 7: Compute $\hat{\mathbf{J}}_{\mathbf{F}_i}(\boldsymbol{\beta}_i^{(k)})$ (cf. (11)).
 - 8: **end for**
 - 9: Update $\hat{\boldsymbol{\alpha}} = [\boldsymbol{\alpha}_1, \dots, \boldsymbol{\alpha}_{N_{\text{dd}}}]$.
 - 10: Compute $\mathbf{r}^{(k),(j)} = \mathbf{P}\hat{\boldsymbol{\alpha}} + \mathbf{Q}\hat{\boldsymbol{\beta}}_i^{(k)}$ and $\nabla_{\mathbf{r}}^{(k),(j)} = \mathbf{P}\hat{\mathbf{J}}_{\mathbf{F}} + \mathbf{Q}$.
 - 11: Compute $\hat{\boldsymbol{\beta}}^{(k+1)} = \hat{\boldsymbol{\beta}}^{(k)} - (\nabla_{\mathbf{r}}^{(k),(j)})^\dagger \mathbf{r}^{(k),(j)}$.
 - 12: **if** $\|\hat{\boldsymbol{\beta}}^{(k+1)} - \hat{\boldsymbol{\beta}}^{(k)}\|_2 < tol \|\hat{\boldsymbol{\beta}}^{(k)}\|_2$ **then**, BREAK
 - 13: **end if**
 - 14: **end for**
 - 15: Update $\mathbf{U}_i^{(j-1)}$ and $\mathbf{W}_i^{(j-1)}$ for $i = 1, \dots, N_{\text{dd}}$ to be used at line 6.
 - 16: Update $\hat{\boldsymbol{\alpha}}$ s.t. $\hat{\boldsymbol{\alpha}}_i = \hat{\mathbf{F}}_i^{(j)}(\hat{\boldsymbol{\beta}}_i)$ to be used at line 6.
 - 17: Store $\hat{\mathbf{U}}_i^{(j)} = \mathbf{Z}_i^{\text{b}}\hat{\boldsymbol{\alpha}}_i + \mathbf{Z}_i^{\text{p}}\hat{\boldsymbol{\beta}}_i$ for $i = 1, \dots, N_{\text{dd}}$.
 - 18: Save $\hat{\boldsymbol{\beta}}^{(0)} = \hat{\boldsymbol{\beta}}$.
 - 19: **end for**
 - 20: Return $\left\{ \hat{\mathbf{U}}_1^{(j)} \right\}_{j=1}^{J_{\text{max}}}, \dots, \left\{ \hat{\mathbf{U}}_{N_{\text{dd}}}^{(j)} \right\}_{j=1}^{J_{\text{max}}}$.
-

$$\hat{\mathbf{J}}_{\mathbf{F}}^{(j)}(\boldsymbol{\beta}) = \text{diag} \left[\hat{\mathbf{J}}_{\mathbf{F}_1}(\boldsymbol{\beta}_1), \dots, \hat{\mathbf{J}}_{\mathbf{F}_{N_{\text{dd}}}}(\boldsymbol{\beta}_{N_{\text{dd}}}) \right], \quad (11a)$$

which is block-diagonal. Each component for $i = 1, \dots, N_{\text{dd}}$ is defined as

$$\hat{\mathbf{J}}_{\mathbf{F}_i}(\boldsymbol{\beta}_i) := - \left(\partial_{\boldsymbol{\alpha}_i} \hat{\mathbf{R}}_i^{(j)} \right)^{-1} \partial_{\boldsymbol{\beta}_i} \hat{\mathbf{R}}_i^{(j)} \Big|_{(\boldsymbol{\alpha}_i, \boldsymbol{\beta}_i) = (\hat{\mathbf{F}}_i^{(j)}(\boldsymbol{\beta}_i), \boldsymbol{\beta}_i)}. \quad (11b)$$

Remark 3. *The Gauss-Newton method solves a least-square problem of size M and requires to fully assemble $\hat{\mathbf{J}}_{\mathbf{F}}$. Therefore, the Gauss-Newton method is expected to be feasible if the dimension of the reduced port spaces is moderate.*

As a reference, we consider in Algorithm 2 the multiplicative overlapping Schwarz method with Dirichlet interface conditions (cf. [7] for the proposed OS procedure for steady PDEs).

Notice that in Algorithm 2 the internal variables come into play in the evaluation of the port-to-bubble maps at line 6 and 7; also, the for loop at lines 5-8 is not parallelizable as opposed to the corresponding loop of the OS2 solver (cf. lines 5-8 in Algorithm 1).

Algorithm 2 Overlapping Schwarz method.

Inputs: $\boldsymbol{\alpha}^{(0)} = [\boldsymbol{\alpha}_1^{(0)}, \dots, \boldsymbol{\alpha}_{N_{\text{dd}}}^{(0)}]$, $\boldsymbol{\beta}^{(0)} = [\boldsymbol{\beta}_1^{(0)}, \dots, \boldsymbol{\beta}_{N_{\text{dd}}}^{(0)}]$ initial conditions, $tol > 0$, maxit .

Outputs: $\left\{ \hat{\mathbf{U}}_1^{(j)} \right\}_{j=1}^{J_{\text{max}}}, \dots, \left\{ \hat{\mathbf{U}}_{N_{\text{dd}}}^{(j)} \right\}_{j=1}^{J_{\text{max}}}$.

- 1: Set $\hat{\boldsymbol{\beta}}^{(0)} = \boldsymbol{\beta}^{(0)}$ and $\hat{\boldsymbol{\alpha}}^{(0)} = \boldsymbol{\alpha}^{(0)}$.
 - 2: **for** $j = 1, \dots, J_{\text{max}}$ **do**
 - 3: **for** $k = 1, \dots, \text{maxit}$ **do**
 - 4: Initialize $\hat{\boldsymbol{\alpha}}^{(k)} = \hat{\boldsymbol{\alpha}}^{(k-1)}$ and $\hat{\boldsymbol{\beta}}^{(k)} = \hat{\boldsymbol{\beta}}^{(k-1)}$.
 - 5: **for** $i = 1, \dots, N_{\text{dd}}$ **do**
 - 6: Update $\hat{\boldsymbol{\beta}}_i^{(k)} \in \arg \min_{\boldsymbol{\beta} \in \mathbb{R}^m} \sum_{g \in \text{Neigh}_i} \|W_i^{\text{p}} \boldsymbol{\beta} - Z_g^{\text{b}} \hat{\mathbf{F}}_g^{\text{eq},(j)}(\hat{\boldsymbol{\beta}}_g^{(k)}) - W_g^{\text{p}} \hat{\boldsymbol{\beta}}_g^{(k)}\|_{L^2(\Gamma_{i,g})}^2$.
 - 7: Update $\hat{\boldsymbol{\alpha}}_i^{(k)} = \hat{\mathbf{F}}_i^{\text{eq},(j)}(\hat{\boldsymbol{\beta}}_i^{(k)})$.
 - 8: **end for**
 - 9: **if** $\|\hat{\boldsymbol{\beta}}^{(k)} - \hat{\boldsymbol{\beta}}^{(k-1)}\|_2 < tol \|\hat{\boldsymbol{\beta}}^{(k)}\|_2$ **then**, BREAK
 - 10: **end if**
 - 11: **end for**
 - 12: Update state and internal variables at iteration $j - 1$ (for evaluation of $\hat{\mathbf{F}}_i^{\text{eq},(j)}$ at line 6 and 7).
 - 13: Store $\hat{\mathbf{U}}_i^{(j)} = \mathbf{Z}_i^{\text{p}} \hat{\boldsymbol{\alpha}}_i^{(k)} + \mathbf{Z}_i^{\text{b}} \hat{\boldsymbol{\beta}}_i^{(k)}$ for each $i = 1, \dots, N_{\text{dd}}$.
 - 14: **end for**
-

4 Numerical results

The FE discretization is characterized by $N_{\text{int}}^{\text{e}} = 1120$ and $N_{\text{ext}}^{\text{e}} = 3960$ elements. We adopt structured meshes in the archetype components that enable logarithmic-in- N_{ℓ}^{v} FE interpolations. In all the numerical results we consider FE polynomial degree $\mathbf{p} = 2$ for displacement, pressure and temperature. The FE space \mathcal{X} and the spaces $\mathcal{X}_{\ell}^{\text{a}}$ are equipped with the weighted inner product

$$(\underline{U}, \underline{U}') = \sum_{d=1}^2 \frac{1}{\lambda_{u_d}} (\underline{u}_d, \underline{u}'_d)_{H^1(\Omega)} + \frac{1}{\lambda_{\text{p}}} (p_{\text{w}}, p'_{\text{w}})_{H^1(\Omega)} + \frac{1}{\lambda_{\text{t}}} (T, T')_{H^1(\Omega)}. \quad (12)$$

In the case of the global space \mathcal{X} , we consider as coefficients $\lambda_{u_1}, \lambda_{u_2}, \lambda_{\text{p}}, \lambda_{\text{t}}$ the largest eigenvalues of the Gramian matrices $\mathbf{C}^{\text{ux}}, \mathbf{C}^{\text{uy}}, \mathbf{C}^{\text{p}}, \mathbf{C}^{\text{t}}$ associated to horizontal and vertical displacement, pressure and temperature, respectively. In the case of the local archetype components, we choose scaling factors $\lambda_{u_1}, \lambda_{u_2}, \lambda_{\text{p}}, \lambda_{\text{t}}$ based on the order of magnitude of the state variables $(u_x, u_y, p_{\text{w}}, T)$ in the global solution at final time J_{max} and at $\bar{\mu} = [1.088 \cdot 10^3, 0.3, 21.33, 0.4558]^T$

(which is the centroid of the training set). These choices are motivated by the need for properly taking into account the contributions of displacement, pressure and temperature, which are characterised by different magnitudes. The monolithic structured mesh is characterized by $N^e = 16896$ elements. We consider a vector of four non-dimensional parameters: the Young's modulus E_Y and the Poisson's ratio ν in the region UA (cf. Figure 1(a)), the thermic factor τ and the constant C_{al} in the detailed mathematical formulation in [7](section 4.2). For all parameters, we construct the non-dimensional parameter domain \mathcal{P} by considering variations of $\pm 8\%$ with respect to the nominal values of E_Y, ν, τ and C_{al} reported in [7, Table 4]: the centroid of the parametric set \mathcal{P} is given by $\mu = \bar{\mu}$.

We train the CB-ROM based on $n_{\text{train}} = 10$ global parameters in $\Xi_{\text{train}} = \{\mu^{(k)}\}_{k=1}^{n_{\text{train}}}$ such that

$$\begin{aligned} \left(E_Y^{(k)}, \nu^{(k)}, C_{\text{al}}^{(k)}, \tau^{(k)} \right) &\stackrel{\text{iid}}{\sim} \text{Uniform}([928.1416, 1.0896 \cdot 10^3] \times [0.2760, 0.3240] \\ &\times [4.9066, 5.7600] \times [0.4193, 0.4922]), \end{aligned} \quad (13)$$

and

$$Q_a^{(k)} \stackrel{\text{iid}}{\sim} \text{Uniform}(\{2, \dots, 7\}),$$

where the role of the parameters $E_Y^{(k)}, \mu_1^{(k)}, C_{\text{al}}^{(k)}, \tau^{(k)}$ in system (1) is specified in [7]. We assess performance based on $n_{\text{test}} = 5$ out-of-sample global parameters $\Xi_{\text{test}} = \{\tilde{\mu}^{(k)}\}_{k=1}^{n_{\text{test}}}$ generated by the same distribution (13). The non-dimensional time interval $(0, t_f]$ is divided into $J_{\text{max}} = 20$ uniform time steps of length $\Delta t = 0.05$; the high-fidelity solutions are stored in the training phase at sampling times in $\mathbf{I}_s \subseteq \{1, \dots, J_{\text{max}}\}$. We set $|\mathbf{I}_s| = 20$ and the same values for the computation and saving time-steps $\Delta t_s = \Delta t = 0.05$. In view of the assessment, we also define the PoU $\{\phi_i\}_{i=1}^{N_{\text{dd}}} \subset \text{Lip}(\Omega; \mathbb{R})$ associated with the partition $\{\Omega_i\}_{i=1}^{N_{\text{dd}}}$ such that

$$\sum_{i=1}^{N_{\text{dd}}} \phi_i(x) = 1, \quad \begin{cases} 0 \leq \phi_i(x) \leq 1 & \forall x \in \Omega, \\ \phi_i(x) = 0 & \forall x \notin \Omega_i, \end{cases} \quad i = 1, \dots, N_{\text{dd}}.$$

Given $\underline{u} \in \mathcal{X} := \bigotimes_{i=1}^{N_{\text{dd}}} \mathcal{X}_i$, we define the Partition of Unity operator

$$\mathbf{P}_{\text{pu}}[\underline{u}] := \sum_{i=1}^{N_{\text{dd}}} \phi_i \underline{u}_i \in H^1(\Omega). \quad (14)$$

We define the out-of-sample average prediction error:

$$E := \frac{1}{n_{\text{test}}} \sum_{\mu \in \Xi_{\text{test}}} \frac{\sqrt{\sum_{j=1}^{J_{\text{max}}} (t^{(j)} - t^{(j-1)}) \|\mathbf{P}_{\text{pu}}[\underline{U}^{(j)}] - \mathbf{P}_{\text{pu}}[\widehat{\underline{U}}^{(j)}]\|_{\mathcal{X}}^2}}{\sqrt{\sum_{j=1}^{J_{\text{max}}} (t^{(j)} - t^{(j-1)}) \|\mathbf{P}_{\text{pu}}[\underline{U}^{(j)}]\|_{\mathcal{X}}^2}}, \quad (15)$$

where $\{\widehat{\underline{U}}^{(j)}\}_j$ is found by solving a ROM by OS2 method. We present the best-fit error

$$E^{\text{bf}} := \frac{1}{n_{\text{test}}} \sum_{\mu \in \Xi_{\text{test}}} \frac{\sqrt{\sum_{j=1}^{J_{\text{max}}} (t^{(j)} - t^{(j-1)}) \|\mathbf{P}_{\text{pu}}[\underline{U}^{(j)}] - \widehat{\underline{U}}_{\text{bf}}^{(j)}\|_{\mathcal{X}}^2}}{\sqrt{\sum_{j=1}^{J_{\text{max}}} (t^{(j)} - t^{(j-1)}) \|\mathbf{P}_{\text{pu}}[\underline{U}^{(j)}]\|_{\mathcal{X}}^2}}, \quad (16)$$

$$\widehat{\underline{U}}_{\text{bf}}^{(j)} = \Pi_{\mathcal{Z}_{\text{glo}}} \mathbf{P}_{\text{pu}}[\underline{U}^{(j)}] \quad (17)$$

where we denote the globally-defined reduced space as $\mathcal{Z}_{\text{glo}} = \text{span}\{\mathbf{P}_{\text{pu}}[\underline{\zeta}_i \circ \Phi_i^{-1}] : \underline{\zeta}_i \in \mathcal{Z}_{L_i}^{\text{a,b}} \cup \mathcal{Z}_{L_i}^{\text{a,p}}, i = 1, \dots, N_{\text{dd}}\}$.

In Figure 2a we show the state estimation error (15) between the solution found by OS2 ROM with HF quadrature and the high-fidelity solution (which is computed by OS2 method with HF solve). Also the best-fit error (16) is depicted with respect to increasing values of bubble and port modes ($m = n$). In Figure 2b we depict the average (in time and over the test parameters) values of the objective functions at Gauss-Newton convergence (cf. line 12) in Algorithm 1). We set $\text{tol} = 10^{-5}$ in Algorithm 1 and we set a threshold for the objective function value equal to 10^{-11} . We consider the same termination criterion for the Gauss-Newton solver and the OS solver; for the solution of port-to-bubble maps, we set a Newton's tolerance of 10^{-9} . For the hyper-reduced OS2, we set an empirical quadrature tolerance of $\text{tol}_{\text{eq}} = 10^{-12}$, which corresponds to the sampling of approximately 19% of elements in the internal component $\Omega_{\text{int}}^{\text{a}}$ and 4% of elements in the external component $\Omega_{\text{ext}}^{\text{a}}$. The OS2 method endowed with empirical

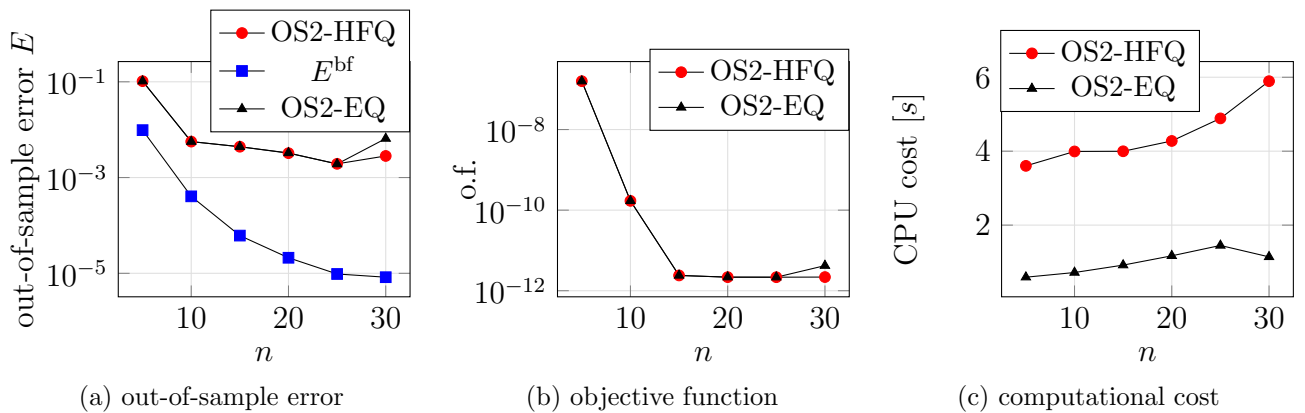


Figure 2: Performance of the OS2 method compared to solution projection for increasing dimensions of the local port and bubble reduced bases ($m = n$).

quadrature on the port-to-bubble maps achieves an out-of-sample prediction accuracy of 0.3% for $n = 15$; the corresponding average time cost is around 1/4 of the cost associated with high-fidelity quadrature. We notice in 2a that for increasing values of n , the error decay of OS2 is significantly slower than the one associated with the best-fit error: we conjecture that this behaviour might be related to the coupling of very dissimilar scales in Algorithm 1. Nevertheless, the average value of the objective function at optimality (cf. figure 2b) demonstrates good convergence properties of the OS2 procedure in Algorithm 1. We also compute the speed-up factor of the hyper-reduced OS2 solver with respect to the monolithic P2-HF solve for $\mu \in \Xi_{\text{test}}$: we find an average value of 212 for $n = 15$ and $m = n$. Figure 3 shows (for $n = 15$ and $m = n$) the decay of the average value of the objective function in a predictive case until the termination criterion is met. The largest number of OS iterations corresponds to the first time steps; furthermore, OS2 seems to require many fewer iterations (for all the time steps) than OS and to achieve a better accuracy in the minimization process.

5 Conclusions

In this work we developed and numerically validated the one-shot overlapping Schwarz (OS2) approach to component-based MOR for time-dependent nonlinear coupled problems (in partic-

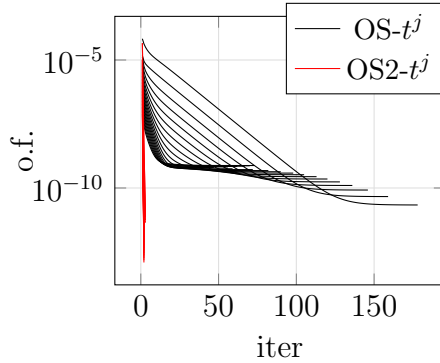


Figure 3: Convergence of OS and OS2 (without hyper-reduction) for time steps $j = 1, \dots, J_{\max}$ and for a fixed dimension of the bubble reduced spaces $n = 15$ and $m = n$.

ular, thermo-hydro-mechanical (THM) systems arising in radioactive waste applications). This work reads as a prolongation of [8]: we extended the OS2 formulation to unsteady problems and we devised a specialized implementation to deal with internal variables. For the THM problem of interest, the developed method reduces online costs by a factor in the range of $[1.7, 4.11] \cdot 10^2$ compared to a standard monolithic FE model with a prediction error of the order of 0.3% (for $n = m = 15$), and resorting to no parallelization of the online ROM solver.

We aim to extend the approach in several directions. We aim at better exploiting the connection between the proposed OS2 method and the (multiplicative or additive) overlapping Schwarz method in particular for nonlinear and time-dependent problems. Also, we aim at combining our approach with the recently-developed OS method discussed in [9]. We wish to devise localized training techniques to avoid the solution to global HF problems at the training phase: we aim to extend the approach in [13] to unsteady PDEs with internal variables. Also, we would investigate the possibility of generalizing our approach to non-overlapping decompositions (cf. [2],[3]): this would enable the coupling of different physical models in different subdomains. Finally, as in a recent work in [10], we aim to combine projection-based ROMs with data-driven methods for multi-scale problems: machine-learning techniques would mitigate the computational effort in domain regions where accuracy constraints usually require intensive FE simulations.

Acknowledgments

The authors acknowledge the financial support of Andra (National Agency for Radioactive Waste Management) and thank Dr. Marc Leconte and Dr. Antoine Pasteau (Andra) for fruitful discussions. The authors also thank Dr. Irina K. Tezaur (Sandia National Laboratories) for her pertinent and useful comments on this work. The authors also acknowledge the support by European Union’s Horizon 2020 research and innovation programme under the Marie Skłodowska-Curie Actions, grant agreement 872442 (ARIA).

REFERENCES

- [1] A. Benaceur and A. Patera. Port-reduced reduced-basis component method for steady state navier–stokes and passive scalar equations. 2022.
- [2] M. Gunzburger, J. Peterson, and H. Kwon. An optimization-based domain decomposition

- method for partial differential equations. *Computers and Mathematics with Applications*, 37(10):77–93, 1999.
- [3] M. D. Gunzburger and H. K. Lee. An optimization-based domain decomposition method for the navier-stokes equations. *SIAM Journal on Numerical Analysis*, 37(5):1455–1480, 2000.
- [4] J. S. Hesthaven, G. Rozza, and B. Stamm. *Certified reduced basis methods for parametrized partial differential equations*, volume 590. Springer, 2016.
- [5] C. Hoang, Y. Choi, and K. Carlberg. Domain-decomposition least-squares petrov–galerkin (DD-LSPG) nonlinear model reduction. *Computer Methods in Applied Mechanics and Engineering*, 384:113997, 2021.
- [6] D. B. P. Huynh, D. J. Knezevic, and A. T. Patera. A static condensation reduced basis element method: approximation and a posteriori error estimation. *ESAIM: Mathematical Modelling and Numerical Analysis*, 47(1):213–251, 2013.
- [7] A. Iollo, G. Sambataro, and T. Taddei. An adaptive projection-based model reduction method for nonlinear mechanics with internal variables: Application to thermo-hydro-mechanical systems. *International Journal for Numerical Methods in Engineering*, 123(12):2894–2918, 2022.
- [8] A. Iollo, G. Sambataro, and T. Taddei. A one-shot overlapping schwarz method for component-based model reduction: application to nonlinear elasticity. *Computer Methods in Applied Mechanics and Engineering*, 404:115786, 2023.
- [9] A. Mota, I. Tezaur, and G. Phlipot. The schwarz alternating method for transient solid dynamics. *International Journal for Numerical Methods in Engineering*, 123(21):5036–5071, 2022.
- [10] E. Parish, P. Lindsay, T. Shelton, and J. Mersch. Embedded symmetric positive semi-definite machine-learned elements for reduced-order modeling in finite-element simulations with application to threaded fasteners. *arXiv preprint arXiv:2307.05434*, 2023.
- [11] A. Quarteroni, A. Manzoni, and F. Negri. *Reduced basis methods for partial differential equations: an introduction*, volume 92. Springer, 2015.
- [12] G. Sambataro. *Component-based model order reduction procedures for large scale THM systems*. PhD thesis, University of Bordeaux, 2022.
- [13] K. Smetana and T. Taddei. Localized model reduction for nonlinear elliptic partial differential equations: localized training, partition of unity, and adaptive enrichment. *SIAM Journal on Scientific Computing*, 45(3):A1300–A1331, 2023.
- [14] T. Taddei and L. Zhang. A discretize-then-map approach for the treatment of parameterized geometries in model order reduction. *Computer Methods in Applied Mechanics and Engineering*, 384:113956, 2021.